Journal of
Intelligent Material
Systems and Structures

Original Article

Journal of Intelligent Material Systems and Structures
2019, Vol. 30(3) 371–385

DOI: 10.1177/1045389X18810803
journals.sagepub.com/home/jim
SAGE

Reference-free damage localization in time-space domain for structural health monitoring of X-COR sandwich composites

Guoyi Li and Aditi Chattopadhyay

Abstract

This article presents a guided wave based damage localization framework using a time-space analysis for structural health monitoring of X-COR sandwich composites with a reference-free perspective to overcome the difficulty in detecting reflected guided waves in a highly attenuated media. Transducers, including macro-fiber composites and piezoelectric wafers, are used to design the sensing paths. The time-space domain is constructed using de-noised signals that are processed by signal processing techniques including matching pursuit decomposition and Hilbert transform. The localization framework is then validated across a wide range of excitation frequencies in X-COR sandwich composites with seeded facesheet delamination. The results indicate that time-space analysis offers a high accuracy for detection and localization of internal damages and serves as a promising framework for structural health monitoring of complex sandwich composites with reinforcements. This work also provides a comprehensive study of the changes in group velocities, attenuation tendencies, and time-space resolution of actuated and converted modes under different excitation frequencies across a range of ultrasonic transducer sizes, thereby helping to improve reliability and accuracy of damage localization in time-space domain.

Keywords

Ultrasonic guided wave, structural health monitoring, X-COR sandwich composite, time-space representation, damage localization, facesheet delamination, converted wave mode

Introduction

Sandwich composites are well suited for mechanical and aerospace applications due to their inherent light weight and excellent durability, strength, stiffness, damping, and impact properties (Du and Jiao, 2009; O'Brien and Paris, 2002). X-COR sandwich composites also possess additional through-thickness reinforcements provided by carbon pins that form a truss-like structure within the foam core while penetrating the facesheets and improving the compressive strength in through-thickness direction, especially when compared with regular foam core sandwich composite structures (Li et al., 2009). Despite the foregoing benefits, the material heterogeneity and complex damage modes, such as facesheet delamination and foam core separation, limit the operational reliability of such material systems (O'Brien and Paris, 2002). Widespread use of X-COR sandwich composite is further limited due to the difficult-to-detect damage scenarios associated with these structures. The low-density foam core, including honeycomb cell and polyurethane foam, has the capacity for higher energy absorption when compared to typical metallic and composite structures (Li et al., 2016; Zhang et al., 2014). Furthermore, the sharp interface between the foam core and the facesheets, due to differences in material properties (i.e. stiffness and density), induces more energy reflection and dissipation, especially when compared to composites without such an interface (Diamanti et al., 2005). These observed characteristics, thus, dramatically increase the difficulty level of energy transmission in the interrogated media and subsequently complicate the information interpretation process in a structural health monitoring (SHM) framework (Cawley, 2018), in both active and passive monitoring systems. To date, limited research has been

School for Engineering of Matter, Transport and Energy, Arizona State University, Tempe, AZ, USA

Corresponding author:
Aditi Chattopadhyay, School for Engineering of Matter, Transport and Energy, Arizona State University, Tempe, AZ 85287-6106, USA.
Email: aditi@asu.edu

devoted to addressing these challenges. Therefore, there is a need to develop reliable and effective SHM techniques with the capability of detecting and localizing internal damage to better leverage the advantages offered by this class of sandwich composite structures.

Ultrasonic guided wave (UGW) based techniques (Chang et al., 2011; Gao et al., 2017; Mohseni and Ng, 2018; Ong et al., 2017) have seen extensive applications for their ability to interrogate large areas, including the through-thickness direction in plate-like structures, and their sensitivity to detect multiple damage types, locations, and severities in various materials (Raghavan and Cesnik, 2007; Revel et al., 2013). As such, several studies have been conducted for the development of UGW based damage identification and localization algorithms (Kessler et al., 2002; Su et al., 2006). The ellipse-based algorithm (Su et al., 2006), which is one of the most popular damage localization methods, compares the difference between the number of UGW modes received by the healthy media (known as a baseline) and damaged media, and identifies the mode(s) that are reflected from the structural discontinuity (i.e. reflected mode) in addition to the mode transmitted from the actuator directly (i.e. actuated mode). Based on the time-of-flight (ToF) information between actuated and reflected modes, ellipses comprising all possible damage locations are constructed and the intersection(s) of these ellipses are regarded as potential damage site(s). The ellipse-based method provides high accuracy and ease of algorithm development; thus, it is widely used for identifying damage locations in the media that possess relatively low energy dissipation such as crack in aluminum plates (Lu et al., 2006). It has been shown that with an appropriate temperature compensation algorithm for group velocity calibration, the localization accuracy of the ellipse-based method can be further improved (Neerukatti et al., 2016a). The Delta-T method, which uses ToF information, has attracted significant interest, particularly for civil applications in the UGW based SHM community. This method is especially noted for its ability to map arrival wave modes covering a large inspection area while maintaining detection accuracy (Ng et al., 2017). However, such methods will work only in the presence of reflected wave modes, where the UGW interacts with the damage and sensors can record the reflected wave modes. They are not applicable to cases where the damage does not lead to reflected wave modes, as in the current problem where facesheet delamination and foam core separation do not cause in-plane discontinuities (in the plane of actuation and sensing). The high level of energy absorption introduced by the foam core and the pins further complicates these issues.

For detecting less-severe damage such as delaminations in composite material systems, alternative techniques such as artificial neural network (ANN) (Su and Ye, 2004), image processing (Moriot et al., 2017; Sohn et al., 2011), and frequency–wavenumber domain analysis (Michaels et al., 2011; Ruzzene, 2007) have shown considerable efficacy and accuracy. However, these techniques are inherently cumbersome and impractical for health monitoring and damage detection in X-COR sandwich composites. First, use of ANN requires baseline and validation information from a statistically sufficient number of samples (Su and Ye, 2004), which is infeasible under real-time conditions. A similar limitation applies to the image processing technique as well. Next, frequency–wavenumber analysis, which is a two-dimensional Fourier transform of the time-space domain, requires fine spatial sampling intervals. Since the time-space domain information is generally obtained using a non-contact laser vibrometer (a well-known nondestructive evaluation (NDE) tool (Ruzzene, 2007)), this inherently restricts the adaptation of frequency–wavenumber analysis to a real-time monitoring system. Finally, the aforementioned methods mostly rely on baseline information, which can prove to be impractical in real applications, since a "healthy" baseline sample may have manufacturing induced defects and its condition may change over time due to environmental exposure.

Despite these limitations, frequency–wavenumber and time-space domain analysis offer constructive guidance for developing a real-time SHM framework for X-COR sandwich composites. First, the time-space domain can be used for measuring guided wave velocities (Kim and Chattopadhyay, 2015), which are critical parameters for developing the damage localization framework, and currently are difficult to obtain theoretically due to the complex dispersion behaviors of UGW propagating in X-COR sandwich composites. Second, both time-space and wavenumber–frequency domain analysis have shown that additional wave mode(s), known as converted mode(s), are generated in addition to the wave mode(s) transmitted from the actuator when UGW propagation crosses a delamination (Kim and Sohn, 2007; Okabe et al., 2010). This observation of converted guided wave modes can function as effective indicators of presence of delamination. Prior work on damage detection of X-COR sandwich composites has shown that while the reflected wave mode from damage cannot be detected, the mode conversion phenomenon caused by the presence of facesheet delamination and foam core separation (Neerukatti et al., 2016b) can be easily observed. However, converted wave modes have proven to be effective indicators of facesheet delamination locations (Li and Chattopadhyay, 2018; Li et al., 2017c), yet a comprehensive study of mode conversion–based localization framework is still needed for optimal detection of accuracy and efficiency.

Motivated by the aforementioned research and based on the observation of delamination-induced converted guided wave modes, a reference-free damage

localization framework in time-space domain that interrogates the structural health of X-COR sandwich composites in real-time is presented in the article. A comprehensive study is conducted to evaluate the localization accuracy of the proposed methodology under a wide range of excitation frequencies. The X-COR specimens are manufactured with seeded facesheet delaminations located between the second and third layers of a four-layer top facesheet. Surface-bonded macro-fiber composites (MFCs) and piezoelectric wafer active sensors (PWASs) are then used as sensors and actuators in relatively low- and high-frequency regions, respectively. The complex sensor signals are de-noised using matching pursuit decomposition (MPD) technique, which is a signal processing technique in time–frequency domain, with an adaptive time–frequency dictionary (Liu et al., 2012; Mallat and Zhang, 1993). In addition, Hilbert transform (Giurgiutiu, 2007; Ulrich, 2006) is implemented for isolating guided wave modes and improving the time-space resolution with a relatively sparse sensing architecture. The trajectories of all wave modes present in time-space domain are identified so that the delamination location, which is the origin of converted wave modes, can be obtained. The predicted damage locations are then validated by NDE techniques and show high accuracy. It is important to note that the developed time-space method is independent of the mode velocity and baseline information, thereby eliminating the need for temperature and environment compensation that are critical in guided wave based SHM systems (Neerukatti et al., 2016a; Singh et al., 2016, 2017). In addition, based on the developed method, this article provides a comprehensive understanding of the mode conversion mechanism in the presence of delamination in complex composite sandwich structures under various frequencies and transducers. This framework is anticipated to be a promising tool for UGW based SHM not only for X-COR sandwich composites but also for other complex structures with high-amplitude attenuation.

The remainder of this article is organized as follows. In section "Damage localization using time-space analysis," the methodology of the developed converted wave based damage localization framework is introduced. Then, in section "Experimental setup", the experimental details, including specimen and sensor specifications, sensor deployment, and data acquisition are described, and the predicted damage location is validated via a flash thermography. Next, the localization results are shown with a discussion of observations in section "Results and discussion". The concluding remarks of the current research work are summarized in the "Concluding remarks" section.

Damage localization using time-space analysis

A schematic view of the proposed converted wave mode based damage localization framework is shown in Figure 1. For each sensing path, an excitation signal is applied to the actuator, and the signals are received by a group of evenly distributed sensors. To eliminate the noise induced by the test environment, bonding of transducers, and the data acquisition system, the MPD algorithm utilizes an adaptive dictionary that contains Gaussian-cosine atoms (Chakraborty, 2010; Liu et al., 2012) to extract the harmonic wave modes from the raw signals in the time–frequency domain. Through a Hilbert transform based envelope detection algorithm, the time-space representation can be constructed, and

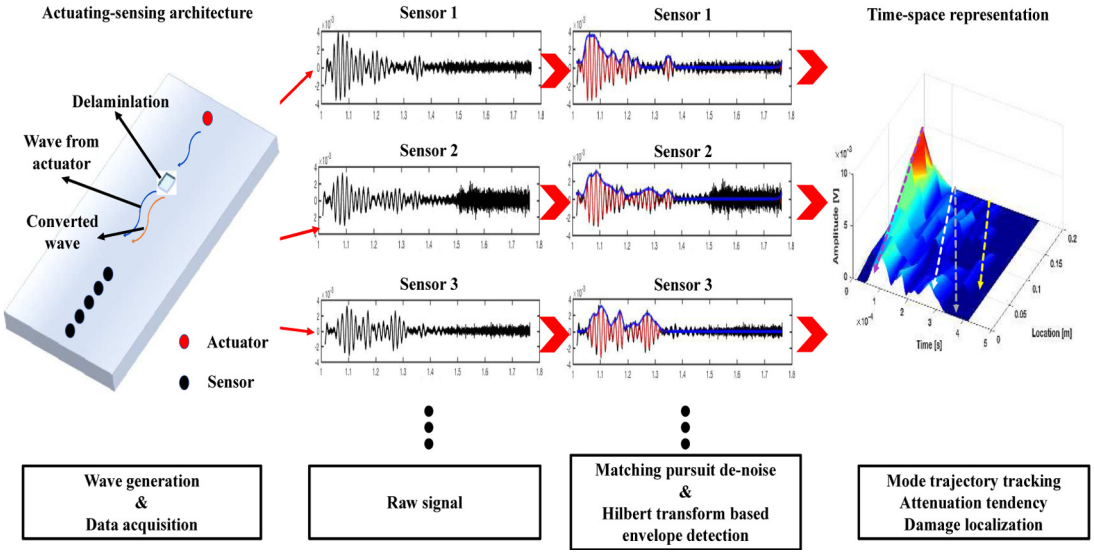

Figure 1. Schematic view of converted wave mode–based damage localization in time-space domain.

trajectories of wave modes can then be identified. A brief introduction of signal de-noising and the time-space representation is presented next.

The signal received by the sensor is defined as $S(x,t)$, where x is the location of the sensor in the sensing path, as shown in Figure 1, and t is the time of UGW propagation. Signal $S(x,t)$ is decomposed by a linear combination of scale–time–frequency basis functions, called atoms in MPD, and the de-noised signal, $S_{de-noised}(x,t)$, is then expressed as

$$S_{de-noised}(x,t) = \sum_{k=0}^{M-1} \alpha_k(x) g_k(x,t) \tag{1}$$

and

$$r_M(x,t) = S(x,t) - \sum_{k=0}^{M-1} \alpha_k(x) g_k(x,t) \tag{2}$$

where $(M-1)$ is the number of iterations, $\alpha_k(x)$ are the coefficients of expansion, $g_k(x,t)$ is the atom function selected from the atom dictionary $\mathbb{D}$ for the kth iteration, and $r_M(x,t)$ represents the residual signal after $(M-1)$th MPD iterations. In order to decompose the signal effectively, while maintaining computational efficiency, the Gaussian-cosine atom dictionary (Chakraborty, 2010) designed based on the excitation signal that was used in the experiments and can be expressed as

$$\mathbb{D} = \left(\frac{8s_l}{\pi}\right)^{1/4} e^{-s_l(t-\tau_n)^2} \cos(2\pi \upsilon_m) \tag{3}$$

where s_l $(l = 1, \ldots, l_{\max})$, τ_n $(n = 1, \ldots, n_{\max})$, and υ_m $(m = 1, \ldots, m_{\max})$ are the parameters controlling scale shift, time shift, and frequency shift, respectively; these variables are used to adjust the waveforms in the dictionary in order to obtain a better signal de-noising performance (Liu et al., 2012). The basis function in each iteration is the atom that has the maximum correlation with the signal $S_{de-noised}(x,t)$ and can be expressed as

$$g_k(x,t) = \underset{g_k(t,s_l,\tau_n,\upsilon_m)\in\mathbb{D}}{\arg\max} \left| \int_{-\infty}^{\infty} r_M(x,t) g_k(t,s_l,\tau_n,\upsilon_m) dt \right| \tag{4}$$

where the expansion coefficient is

$$\alpha_k(x) = \int_{-\infty}^{\infty} r_M(x,t) g_k(x,t) dt \tag{5}$$

As shown in Figure 1, the harmonic waveforms (in red color) contained in sensing signals can be efficiently extracted through the MPD algorithm, while the noise is filtered out due to less correlation with the atoms in the dictionary. A Hilbert-based envelope detection algorithm (Giurgiutiu, 2007; Ulrich, 2006) is then applied to isolate wave modes, which improves the efficiency of the damage localization in the time-space domain. The envelope of the wave mode can be found from the absolute value of the analytical signal, $S_{analytical}(x,t)$, whose real part is defined as the original de-noised signal; the imaginary part is the Hilbert transform of the de-noised signal. The analytical signal can be written as follows

$$S_{analytical}(x,t) = S_{de-noised}(x,t) + i\mathcal{H}(S_{de-noised}(x,t)) \tag{6}$$

where $\mathcal{H}(\cdot)$ is the Hilbert transform that can be expressed as

$$\mathcal{H}(S_{de-noised}(x,t)) = -\frac{1}{\pi} \lim_{\varepsilon \to 0} \int_{\varepsilon}^{\infty} \frac{S_{analytical}(x,t+\tau) - S_{analytical}(x,t-\tau)}{\tau} d\tau \tag{7}$$

The envelope of each UGW mode, $ENV(x,t)$, can be expressed as

$$\begin{aligned} ENV(x,t) &= \left| S_{analytical}(x,t) \right| \\ &= \sqrt{S^2_{de-noised}(x,t) + \mathcal{H}^2(S_{de-noised}(x,t))} \end{aligned} \tag{8}$$

and represents the signals constructed in the time-space domain by the envelopes (i.e. blue lines in Figure 1), thus preserving not only the amplitude information but also the spatial–temporal relationship of wave modes contained in sensing signals. With known spatial information of each sensor, the three-dimensional time-space representation is constructed. It should be observed in Figure 1 that, although multiple modes appear in the time-space domain, the trajectories can be easily tracked by linear regression using time-space information; the slope of the regression line corresponds to the wave mode velocity, and the intersection with the spatial direction at time zero indicates the source location of the wave mode. The reason for using linear regression is the hypothesis that the delamination-induced converted wave still maintains the inherent characteristics of UGW wave mode (e.g. constant group velocity; Giurgiutiu, 2007; Yu and Giurgiutiu, 2005). In addition, the propagation direction of each wave mode is determined by the fact that the amplitude of each wave attenuates with respect to the propagation distance (Li et al., 2017a). This study will focus on the wave mode that propagates in the direction of actuator to sensor(s), defined as forward direction. It should be emphasized that, as the primary advantage of time-space analysis, the top-view of the time-space representation reveals the relation between time and sensor location enabling the spatial domain regression, while the side-view of the time-space representation presents the wave mode

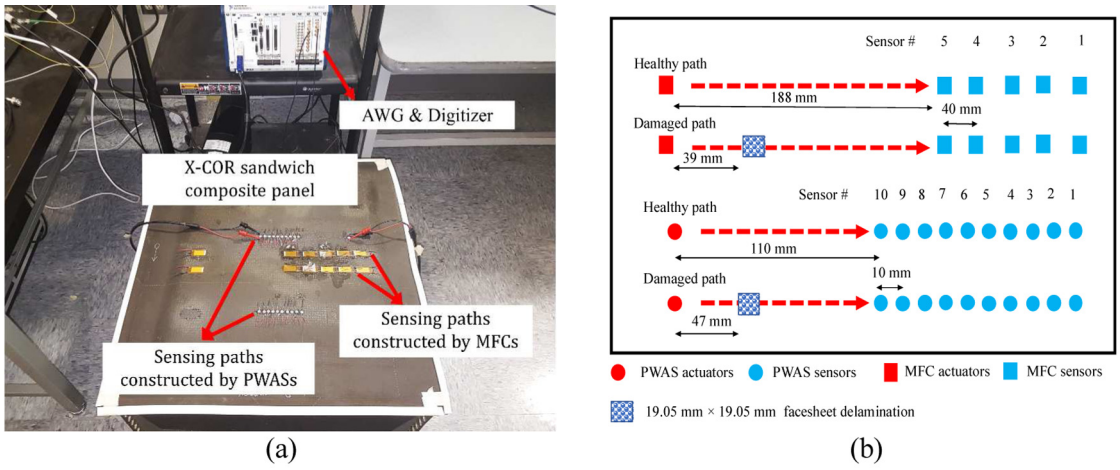

Figure 2. Illustration of (a) experimental setup and (b) schematic view of test plate and sensor deployment.

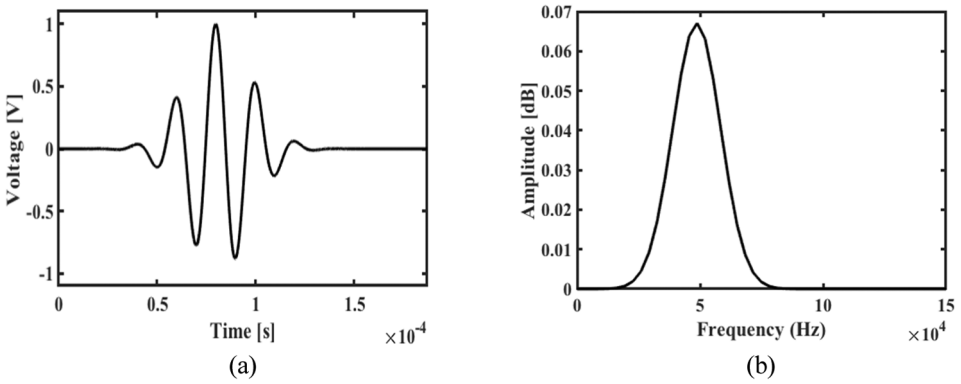

Figure 3. (a) Excitation signal and (b) its frequency spectrum under a 50-kHz excitation frequency.

attenuation tendency, facilitating propagation direction identification.

Experimental setup

X-COR panel configuration and transducer deployment

X-COR sandwich panels for testing were fabricated at the Boeing company facility in Mesa, Arizona, USA, with the dimensions of 450 mm × 450 mm × 13 mm. The facesheets were constructed using a quasi-isotropic layup of prepreg carbon fiber reinforced laminae with the facesheets comprising four layers in the top and eight layers in the bottom surface; the core structure was made of polyurethane foam. In addition, evenly distributed carbon pins at an angle of approximately 20° with respect to the out-of-plane direction penetrate through the foam core, top and bottom facesheets. Based on the critical delamination size of composite structures (Díaz Valdés and Soutis, 2002), single-fold Teflon layer with a size of 19 mm × 19 mm was inserted between the second and third layers of the four-layer top facesheet. The carbon pins were trimmed in the regions of the seeded delaminations to induce structural discontinuities that could simulate interply delamination. A picture of the experimental setup and a schematic view illustrating sensor deployment are shown in Figure 2. A NI PXI 14-bit 100 MS/s arbitrary wave generator (AWG) and a 12-bit 60 MS/s digitizer were used to generate a five-cycle cosine tone burst excitation signal and to collect signals from each sensor with a sampling frequency of 20 MHz, respectively, for the purpose of demonstration. The waveform and its corresponding bandwidth in the frequency domain under a 50-kHz excitation frequency are shown in Figure 3. In order to overcome the limitation posed by transducer's resonance frequency (Peairs et al., 2007) that restricts the range of its effective excitation frequency, MFC transducers and PWASs were bonded to the surface of X-COR panel using superglue for interrogating delamination under 10–100 kHz and 100–1000 kHz frequency ranges, respectively. For the relatively lower frequency region, each sensing path contained an MFC actuator and five 40-mm equally spaced MFC

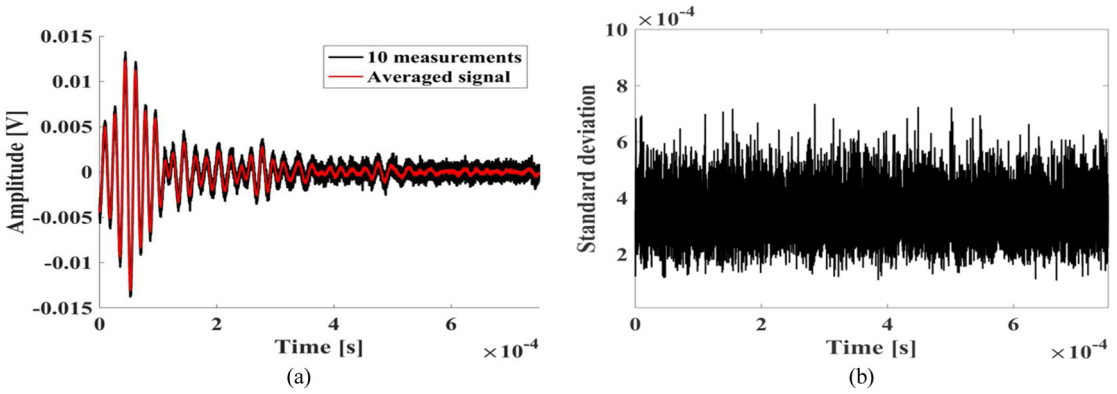

Figure 4. Demonstration of (a) averaged signal associated with 10 measurements and (b) standard deviation with respect to sampling points under 50 kHz.

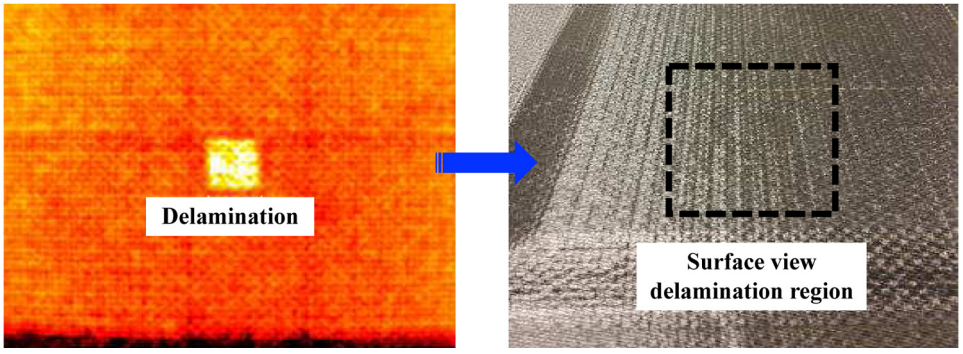

Figure 5. Facesheet delamination detected by flash thermography.

sensors (M 2814 P2, dimensions: 37 mm × 18 mm); for the relatively higher frequency region, each sensing path contained a piezoelectric actuator and 10 10-mm equally spaced PWASs (APC 850 disk, diameter: 6.35 mm). The final recorded signal for each experiment was taken as the average of 10 measurements. As an example, the averaged signal associated with 10 measurements using MFC transducers with a healthy pitch-catch distance of 188 mm under 50 kHz is shown in Figure 4(a), and the corresponding standard deviation of each sampling point is shown in Figure 4(b). The maximum standard deviation was less than 0.001, and the averaged mean square error (MSE), across all sampling points and measurements, was 1.1723×10^{-7}. The formulation of the averaged MSE used in this study can be expressed as

$$MSE = \frac{1}{TW}\sum_{t=0}^{T}\sum_{m=1}^{W}\left(S_{averaged}(t) - S_w(t)\right)^2 \qquad (9)$$

where $S_{averaged}(t)$ is the averaged signal, $S_w(t)$ denotes the wth measurement, W is the number of measurements being averaged, and T is the sample points in each measurement ($T = 15,000$ in this demonstration). It can be seen that the measurements were very consistent, and the experimental noise was reduced by the averaging process.

Validation of delamination size and location using flash thermography

Flash thermography has been used as a validation tool of the proposed damage localization framework. A thermal wave imaging system (EchoTherm) was used to excite the thermal wave through a flash pulse and record response of the X-COR sandwich structure by an infrared camera (Maierhofer et al., 2014). All facesheet delaminations were successfully detected by the flash thermography; the location and size of delamination detected by the thermal imaging were very close to the predefined location and the size of fold Teflon insertion (i.e. 19 mm × 19 mm), ensuring precision of the error analysis that will be discussed in the next section. As a demonstration, one of the thermal images is shown in Figure 5 with the surface view of the delamination region.

Results and discussion

In order to achieve effective excitation, the total number and amplitudes of the modes present in the

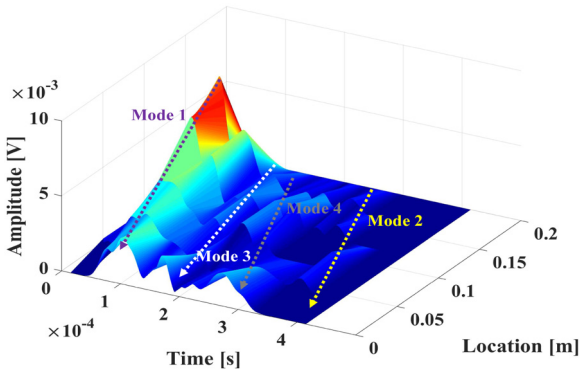

Figure 6. Time-space representation for signals collected from paths with delamination under a 70-kHz excitation frequency.

excitation frequency range of 10–100 kHz and 100–1000 kHz were investigated with MFC transducers and PWASs, respectively. For the sensing path constructed by MFC transducers, the signals with frequencies between 50 and 70 kHz show relatively more wave modes with larger amplitudes compared to other excitation frequencies, indicating higher energy content and more mode information. Through the same process, the suggested excitation region, for the sensing path constructed by PWASs, was found to be between 300 and 400 kHz.

Damage localization using MFC transducers

Based on the excitation ranges obtained through the frequency investigation, time-space analysis is conducted for damage localization with excitation frequencies of 50, 60, and 70 kHz using the sensing path constructed by the MFC transducers. The time-space representation based on the signals received by five MFC sensors under a 70-kHz excitation frequency is presented in Figure 6. It should be emphasized that in

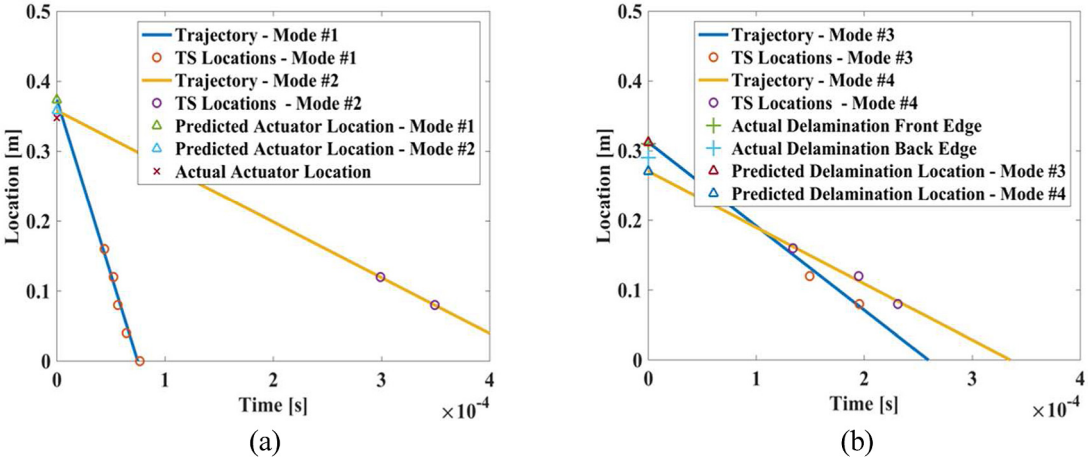

Figure 7. Prediction for (a) actuator and (b) delamination under a 70-kHz excitation frequency (TS: time-space).

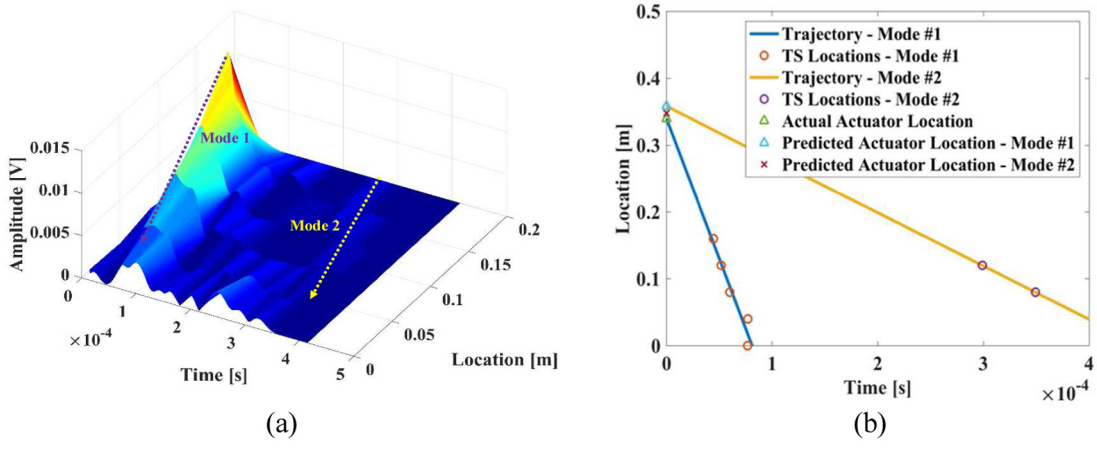

Figure 8. (a) Time-space representation and (b) actuator prediction for healthy path under 70 kHz (TS: time-space).

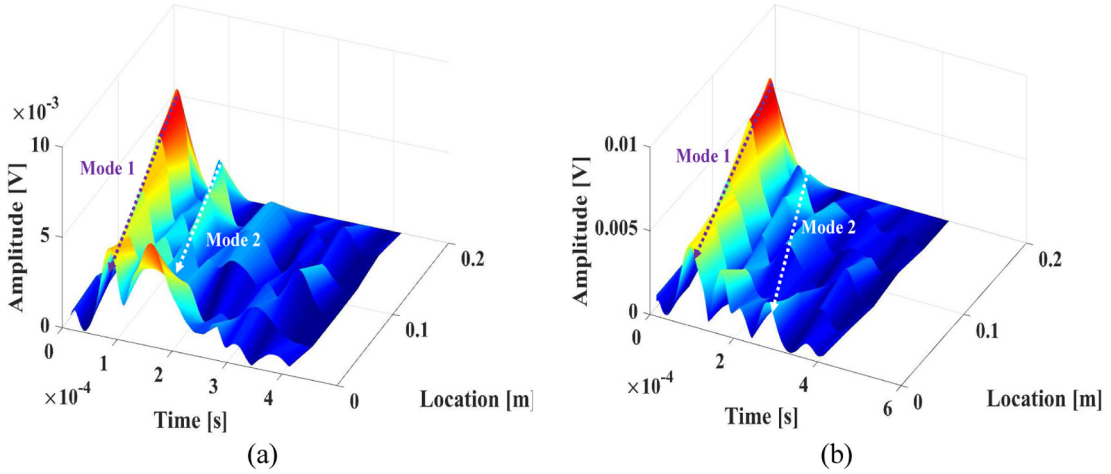

Figure 9. Time-space representation for signals collected from paths with delamination under (a) 50 kHz and (b) 60 kHz excitation frequencies.

all time-space representation shown in this article, the position of the last sensor, which is the farthest sensor in the array from the actuator, is defined as the origin in the space domain. The dashed lines in Figure 6 represent four wave mode trajectories that propagate in the forward direction. Note that the modes that propagate in the opposite direction, which are the reflected waves from the boundaries identified by the mode attenuation analysis, are ignored. Figure 7 shows the four identified mode trajectories in the top view of time-space domain and the predicted actuator and delamination locations for actuated and converted wave modes, respectively. It can be seen that the two actuated wave modes in Figure 7(a) can accurately indicate the location of the actuator, while the two converted wave modes in Figure 7(b) precisely locate the delamination without any baseline information.

To demonstrate that the appearance of converted wave modes is due to the presence of facesheet delamination, in Figure 8(a), the time-space representation of a healthy sensing path containing just two actuated wave modes is shown. The corresponding top-view wave mode trajectories are shown in Figure 8(b). By comparing these trajectories with the trajectories of the actuated wave modes in the path with delamination, shown in Figure 7(a), it can be observed that the converted wave modes are absent in the healthy sensing path and the trajectories of actuated modes are similar. This is an indication that the presence of delamination has minor impact on the trajectory of the actuated mode. The time-space analysis was conducted under an excitation frequency of both 70 kHz and at signals under 50 and 60 kHz excitation frequencies in order to explore the behaviors of actuated and converted wave modes under varying excitation frequencies. The time-space representation and the corresponding localization results of the sensing path with delamination are shown in Figures 9 and 10, respectively. It can be observed that there are two modes, one actuated mode and one converted mode, propagating in the forward direction under both 50 and 60 kHz excitation frequencies, as shown Figure 9(a) and (b), respectively; other modes are reflected waves from the boundaries. As shown in Figure 10(a) and (c), the prediction for the actuator location correlates well with the actual location, and the mode trajectories are similar. The delamination locations are also successfully predicted under both excitation frequencies, as shown in Figure 10(b) and (d). Comparing the trajectories of converted wave modes under 50, 60, and 70 kHz excitation frequencies, it can be seen that all the detected converted wave modes are effective indicators of the presence and location of facesheet delamination, while converted wave modes show different behaviors with varying frequencies.

Damage localization using PWASs

For investigating the proposed localization method in a high-frequency range (>100 kHz), the excitation frequencies of sensing path constructed by PWASs were set to 300, 350, and 400 kHz. The time-space representation constructed by the signals received by 10 equally distributed PWASs under a 350-kHz excitation frequency is presented in Figure 11. Through the time-space analysis, four wave modes that propagate in the forward direction are found (marked by four colors in Figure 11), two of which are proven to be actuated modes (mode 1 and 2), while the other two are the converted wave modes (modes 3 and 4) initiated at the delamination location. From the top view of these four modes shown in Figure 12, it can be seen that the two actuated modes identify the actuator location correctly, while the two converted modes successfully locate delamination.

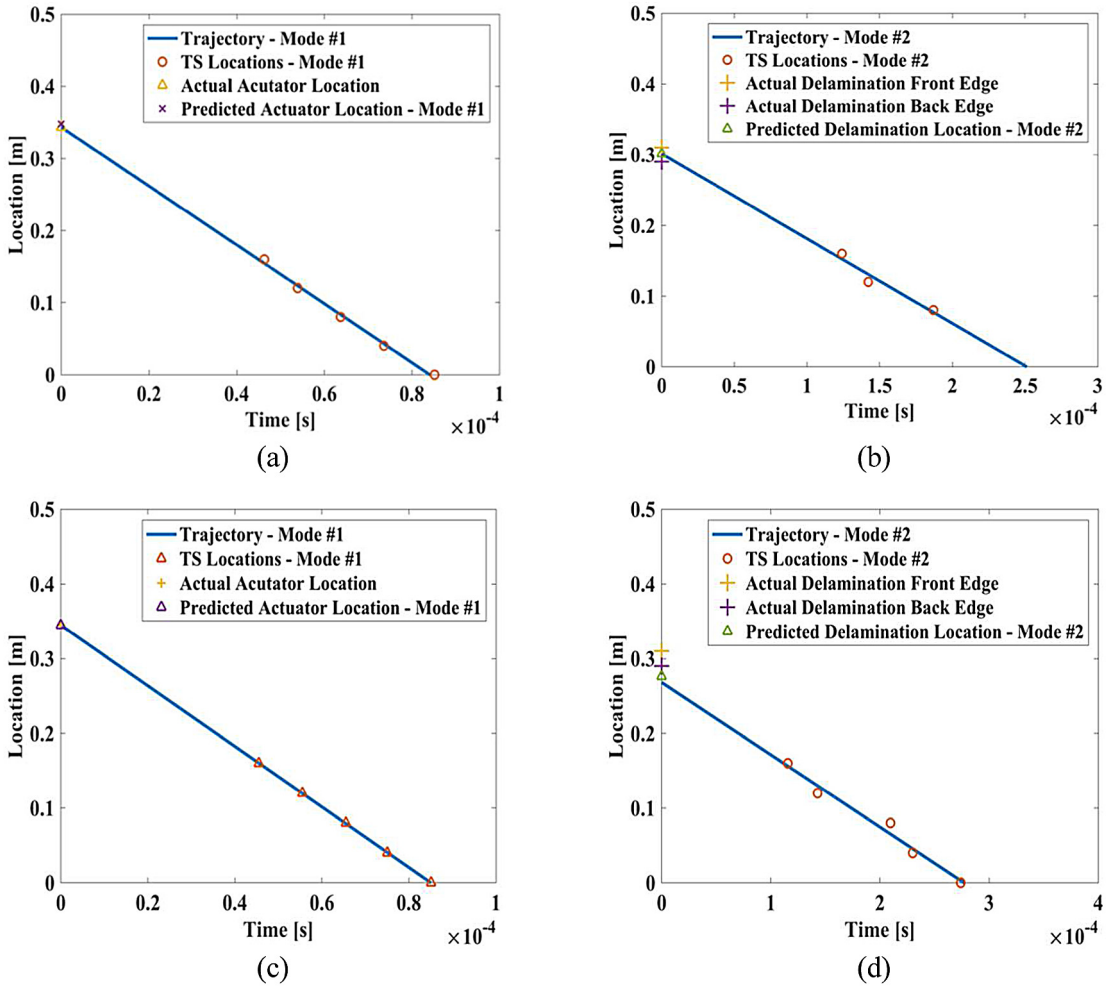

Figure 10. Predictions for actuator locations under (a) 50 kHz and (c) 60 kHz, and predictions for delamination locations under (b) 50 kHz and (d) 60 kHz, (TS: time-space).

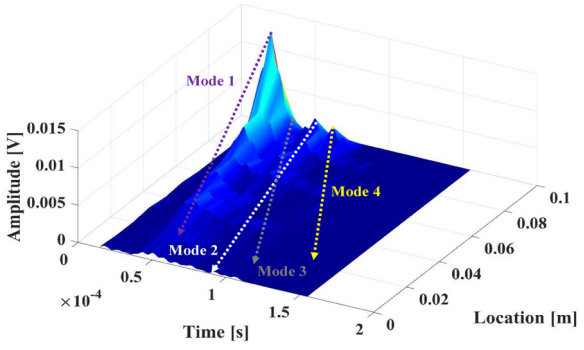

Figure 11. Time-space representation for signals collected from paths with delamination under a 350-kHz excitation frequency.

For the purpose of demonstration, the time-space representation constructed by a healthy sensing path under the same excitation frequency is shown in Figure 13(a). It shows that only the actuated wave modes are present in the time-space domain, and the trajectories of these two modes that are shown in Figure 13(b) correctly indicate the actuator location. Furthermore, the time-space representation of the sensing path with delamination under 300 and 400 kHz excitation frequencies is presented in Figure 14(a) and (b), respectively. Based on the time-space representation, there are four modes propagating in the forward direction under a 300-kHz excitation frequency, including one actuated mode and three converted wave modes, while two modes are found under a 400-kHz excitation frequency, including one actuated mode and one converted wave mode. The trajectories shown in Figure 15(a) to (d) show that the actuated wave modes and converted wave modes can correctly indicate the locations of the actuator and delamination, respectively.

Discussion

Based on the presented localization results, it can be observed that the actuated and converted wave

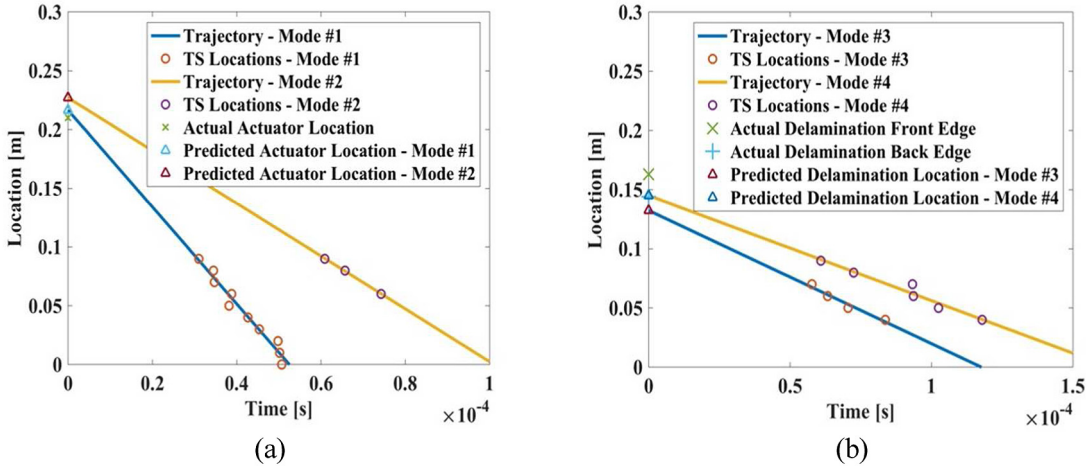

Figure 12. Prediction for (a) actuator and (b) delamination under a 350-kHz excitation frequency (TS: time-space).

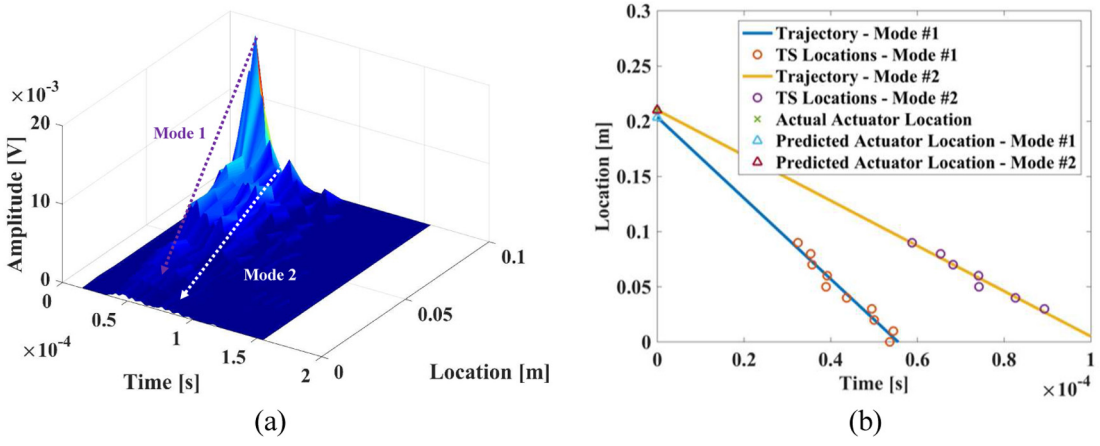

Figure 13. (a) Time-space representation and (b) actuator prediction for healthy path under 350 kHz (TS: time-space).

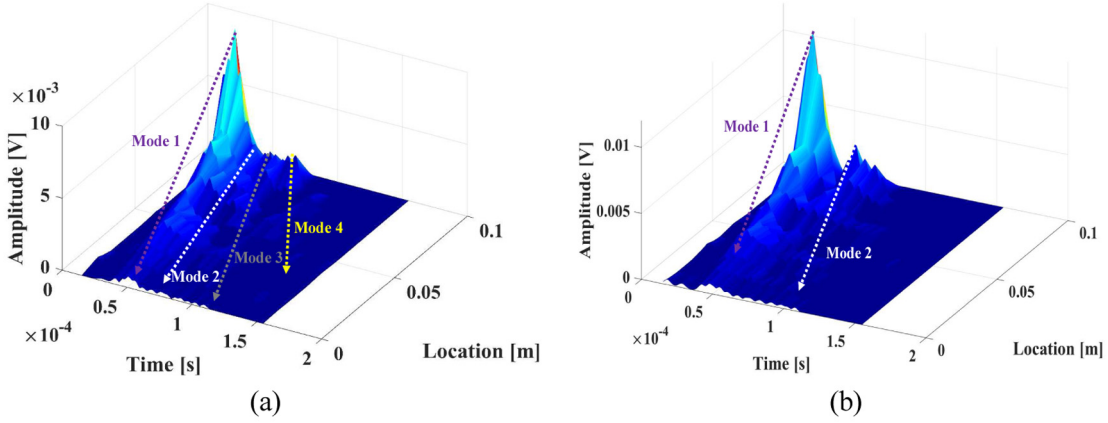

Figure 14. Time-space representation for signals collected from paths with delamination under (a) 300 kHz and (b) 400 kHz excitation frequencies.

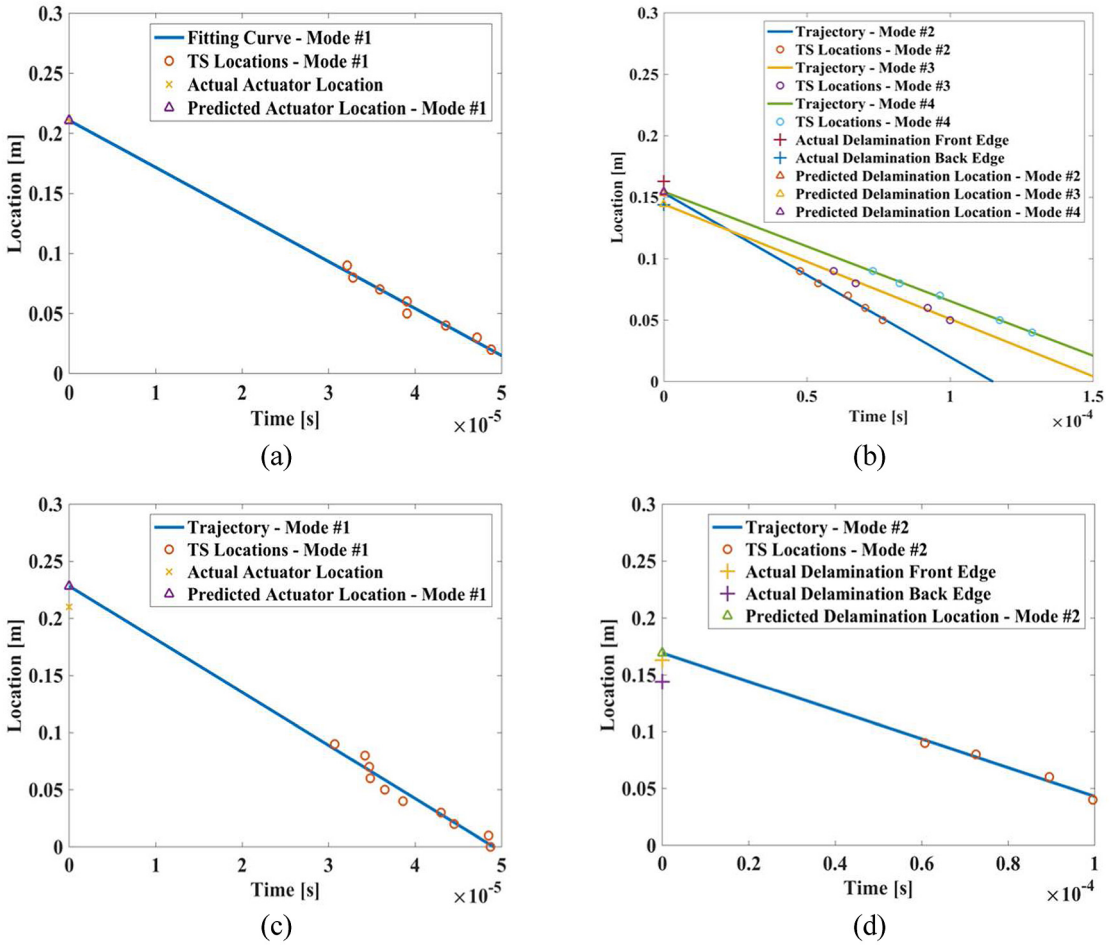

Figure 15. Predictions for actuator locations under (a) 300 kHz and (c) 400 kHz, and predictions for delamination locations under (b) 300 kHz and (d) 400 kHz, (TS: time-space)

Table 1. Error analysis for prediction of actuator location.

Frequency (kHz)	Sensing path	Mode	Pred. Loc (m)	Act. Loc (m)	Error (%)
350	Healthy	Mode 1	0.2036	0.2100	3.05
350	Healthy	Mode 2	0.2101	0.2100	0.05
300	Damaged	Mode 1	0.2108	0.2100	0.38
350	Damaged	Mode 1	0.2165	0.2100	3.10
350	Damaged	Mode 2	0.2270	0.2100	8.10
400	Damaged	Mode 1	0.2283	0.2100	8.71
70	Healthy	Mode 1	0.3396	0.3480	2.41
70	Healthy	Mode 2	0.3582	0.3480	2.93
70	Damaged	Mode 1	0.3735	0.3480	7.33
70	Damaged	Mode 2	0.3582	0.3480	2.93
60	Damaged	Mode 1	0.3447	0.3480	0.95
50	Damaged	Mode 1	0.3434	0.3480	1.32

Pred. Loc: predictive location; Act. Loc: actual location.

modes are able to predict the respective locations of the actuator and the delamination. The errors of all the sensing cases in localizing the actuator and delamination are summarized in Tables 1 and 2, respectively, and the error for each wave mode is defined as

$$\text{Error} = \left| \frac{\text{Predicted location} - \text{actual location}}{\text{Actual location}} \right| \times 100\% \tag{10}$$

It should be noted that, when predicting the location of delamination, if the predicted location is within the

Table 2. Error analysis for prediction of delamination location.

Frequency (kHz)	Sensing path	Mode	Pred. Loc (m)	Act. Loc.Front (m)	Act. Loc.Back (m)	Error (%)
300	Damaged	Mode 2	0.1535	0.1630	0.1440	0.00
300	Damaged	Mode 3	0.1443	0.1630	0.1440	0.00
300	Damaged	Mode 4	0.1545	0.1630	0.1440	0.00
350	Damaged	Mode 2	0.1324	0.1630	0.1440	8.06
350	Damaged	Mode 3	0.1450	0.1630	0.1440	0.00
400	Damaged	Mode 3	0.1692	0.1630	0.1440	3.80
70	Damaged	Mode 3	0.3121	0.3090	0.2900	0.68
70	Damaged	Mode 4	0.2715	0.3090	0.2900	6.38
60	Damaged	Mode 2	0.2682	0.3090	0.2900	7.52
50	Damaged	Mode 2	0.3013	0.3090	0.2900	0.00

Pred. Loc: predictive location; Act. Loc.Front: front edge of delamination; Act. Loc.Back: back edge of delamination.

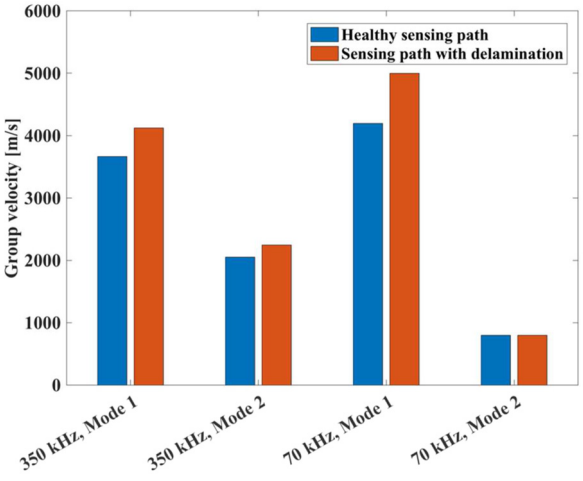

Figure 16. Comparison of group velocities of actuated wave modes between healthy and damaged sensing paths.

real delamination region, the error is zero; if the predicted location is out of the real delamination region, the error will be calculated using equation (10), and the actual location will be regarded as the edge of delamination that is close to the predicted delamination location. For consistency, the wave mode numbers listed in this section are directly associated with the modes identified in the time-space domain as presented in the previous two subsections, while the "healthy" and "damaged" sensing paths refer to the sensing path without and with delamination, respectively. Most of the errors listed in Table 1 are within 3%, indicating that the prediction of actuator location is accurate under varying excitation frequencies. Similarly, the errors in predicting the delamination location, listed in Table 2, indicate that the current time-space framework provides high accuracy in predicting the location of facesheet delamination under a wide range of excitation frequency. In addition, it can be seen that the prediction errors with relatively higher excitation frequencies (300, 350, and 400 kHz) are, generally, smaller than those under relatively lower excitation frequencies (50, 60, and 70 kHz), except for mode 2 under a 350-kHz excitation frequency, which shows a comparable value to those with relatively lower excitation frequencies. The primary reason for this difference is that PWAS provides a better spatial resolution for time-space analysis than MFC due to the size of PWAS used in this study, which as mentioned in the previous section is much smaller than MFC.

Table 3. Group velocities of converted wave modes.

Frequency (kHz)	Converted wave mode	Velocity (m/s)
300	Mode 2	1355
300	Mode 3	933
300	Mode 4	890
350	Mode 2	1125
350	Mode 3	888
400	Mode 2	1262
70	Mode 3	1203
70	Mode 4	809
60	Mode 2	968
50	Mode 2	1200

Group velocities are one of the most important parameters in UGW based damage localization framework and are explored here for both actuated and converted modes. In Figure 16, a comparison of the actuated wave modes between healthy and damaged sensing paths under excitation frequencies of 70 and 350 kHz are presented. It can be observed that the presence of damage has a minor impact on the group velocities of actuated wave modes; the discrepancies between actuated wave mode with and without facesheet delamination are due to the quasi-isotropic characteristic of the carbon fiber composite facesheet, which results in differences in elastic stiffness between sensing paths. The group velocities of all converted modes in this work are listed in Table 3, showing that they vary under different excitation frequencies. It should be emphasized that the fundamental mechanism

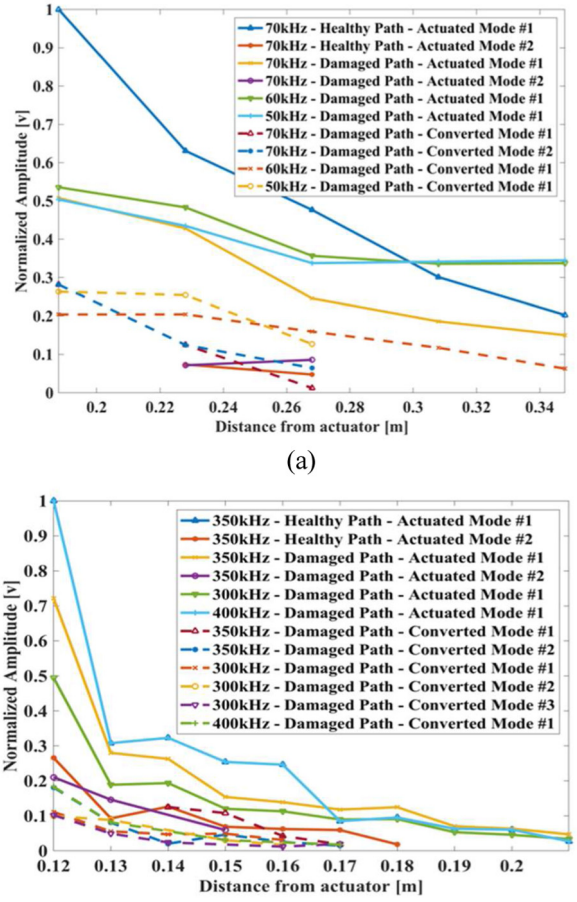

Figure 17. Attenuation tendencies of UGW modes under (a) low-frequency region (50, 60, and 70 kHz) and (b) high-frequency region (300, 350, and 400 kHz).

governing the presence of converted wave mode(s) is that the waves propagate through region(s) with different thicknesses, from where the wave is excited. Thus, although the thickness change, caused by the presence of facesheet delamination, remains the same, the group velocities of converted modes change under different excitation frequencies.

The attenuation tendencies of all the modes under low- and high-frequency regions, as a side-view of time-space domain, are summarized in Figure 17(a) and (b), respectively. From both figures, it can be observed that the amplitudes of actuated wave modes (solid lines) are generally much greater than those of converted wave mode (dash lines) under both low- and high-frequency regions, except for the second actuated modes detected under 70 and 350 kHz from both healthy and damaged sensing paths. This phenomenon can be interpreted as follows: the complex dispersion behaviors (Li et al., 2017b; Neerukatti et al., 2016b) of UGW propagating in X-COR sandwich composites result in multiple modes with various energy content (Srivastava and Lanza di Scalea, 2009) and this fact leads to obtaining two actuated modes with a large amplitude difference under 70 and 350 kHz. By comparing the amplitude difference of actuated wave modes between healthy and damaged paths, there is an obvious reduction found in the amplitude of mode 1 under both 70 and 350 kHz excitation frequencies, indicating that the converted wave modes are formed by a portion of energy from these actuated modes. This affects the accuracy of actuator location prediction as the center of wave modes with lower amplitude are more difficult to detect. For instance, it can be observed in Table 1 that mode 1 of the sensing path with delamination under excitation frequencies of 400 and 70 kHz and mode 2 of the sensing path with delamination under an excitation frequency of 350 kHz show approximately 8% error, which is slightly larger than those without delamination. In addition, the amplitude of both actuated and converted wave modes attenuate much faster under a high excitation frequency suggesting that a better time resolution may be obtained by decreasing the distance between the sensor and the actuator.

Concluding remarks

A converted guided wave based damage localization framework was developed for SHM of X-COR sandwich composites. MFC transducers and PWASs were used to construct the sensing paths under a wide range of excitation frequencies after which the raw signals were de-noised through MPD. Time-space representation was subsequently constructed by the envelopes of de-noised signals, which were identified via a Hilbert transform. Through regression in the time-space domain, the trajectories of damage-induced converted waves were tracked without any baseline information, and the corresponding source locations were then identified, indicating the methodology does not depend on wave mode velocities and temperature. Results suggest that the converted wave modes are effective indicators of the location of the facesheet delaminations. The localization error, including the error in predicting actuator locations using actuated modes, were small as shown through error analyses. In addition, through the investigation of group velocity and amplitude attenuation using the time-space domain, it was found that the converted wave modes (1) contained less energy and attenuated faster than the actuated mode and (2) showed significantly higher attenuation rate at high-frequency excitation regions (>300 kHz). It was also observed that mode conversion behavior was different under various excitation frequencies; however, this had a minor impact on the localization results. Unlike ToF-based methods which rely on reflected waves from the damages, the current method utilizes the mode conversion caused by change in thickness of the delamination region, which leads to additional modes with variations in dispersion characteristics. Future investigations will

focus on incorporating directionality of wave propagation to enable the inspection of two-dimensional anisotropic structures.

Acknowledgements

The authors thank Dr Daniel W. Huff, Technical Monitor, for the support of this work including assistance in preparing the X-COR sandwich panels. In addition, the authors thank student workers, Mr Christopher Sorini and Mr Abhishek Rajadas, for manufacturing the samples at the Boeing facility in Mesa, AZ.

Declaration of conflicting interests

The author(s) declared no potential conflicts of interest with respect to the research, authorship, and/or publication of this article.

Funding

The author(s) disclosed receipt of the following financial support for the research, authorship, and/or publication of this article: This work was supported by the Adaptive Intelligent Materials and Systems (AIMS) Center Industry Consortium Core Project; Co-sponsor: The Boeing Company, Mesa, AZ, USA.

ORCID iD

Guoyi Li https://orcid.org/0000-0002-9228-4236

References

Cawley P (2018) Structural health monitoring: closing the gap between research and industrial deployment. *Structural Health Monitoring* 17: 1225–1244.

Chakraborty D (2010) *Time–frequency based adaptive learning for structural health management*. PhD Thesis, Arizona State University, Tempe, AZ.

Chang F-K, Markmiller JFC, Yang J, et al. (2011) Structural health monitoring. In: Johnson SB, Gormley TJ, Kessler SS, et al. (eds) *System Health Management: With Aerospace Applications*. Hoboken, NJ: John Wiley & Sons, pp. 419–428.

Díaz Valdés SH and Soutis C (2002) Real-time nondestructive evaluation of fiber composite laminates using low-frequency Lamb waves. *Journal of the Acoustical Society of America* 111(5): 2026–2033.

Diamanti K, Soutis C and Hodgkinson JM (2005) Non-destructive inspection of sandwich and repaired composite laminated structures. *Composites Science and Technology* 65(13): 2059–2067.

Du L and Jiao G (2009) Indentation study of Z-pin reinforced polymer foam core sandwich structures. *Composites Part A: Applied Science and Manufacturing* 40(6–7): 822–829.

Gao D, Wu Z, Yang L, et al. (2017) Integrated impedance and Lamb wave based structural health monitoring strategy for long-term cycle-loaded composite structure. *Structural Health Monitoring* 17: 763–776.

Giurgiutiu V (2007) *Structural Health Monitoring: With Piezoelectric Wafer Active Sensors*. Cambridge, MA: Academic Press.

Kessler SS, Spearing SM and Soutis C (2002) Damage detection in composite materials using Lamb wave methods. *Smart Materials and Structures* 11(2): 269.

Kim I and Chattopadhyay A (2015) Guided Lamb wave based structural health monitoring using a novel wave packet tracing method for damage localization and size quantification. *Journal of Intelligent Material Systems and Structures* 26(18): 2515–2530.

Kim SB and Sohn H (2007) Instantaneous reference-free crack detection based on polarization characteristics of piezoelectric materials. *Smart Materials and Structures* 16(6): 2375–2387.

Li G and Chattopadhyay A (2018) Multi-dimensional signal processing and mode tracking approach for guided wave based damage localization in X-COR sandwich composite. *Mechanical Systems and Signal Processing* 109: 134–149.

Li G, Neerukatti RK and Chattopadhyay A (2017a) Ultrasonic guided wave propagation in composites including damage using high-fidelity local interaction simulation. *Journal of Intelligent Material Systems and Structures* 29: 969–985.

Li G, Neerukatti RK, Rajadas A, et al. (2017b) Guided wave based damage assessment in X-COR composite sandwich structures. In: *Proceedings of the 25th AIAA/AHS adaptive structures conference*, Grapevine, TX, January 2017. Reston, VA: American Institute of Aeronautics and Astronautics.

Li G, Rajadas A, Chattopadhyay A, et al. (2017c) A reference-free guided wave based damage localization approach for highly dispersive structures. *Structural Health Monitoring* 1: 1607–1614.

Li Y, Jun X, Tan Y, et al. (2009) Study on compressive properties of X-cor sandwich structures. *Acta Aeronautica et Astronautica Sinica* 30: 557–561.

Li Z, Chen X, Jiang B, et al. (2016) Local indentation of aluminum foam core sandwich beams at elevated temperatures. *Composite Structures* 145: 142–148.

Liu Y, Fard MY, Chattopadhyay A, et al. (2012) Damage assessment of CFRP composites using a time–frequency approach. *Journal of Intelligent Material Systems and Structures* 23(4): 397–413.

Lu Y, Ye L and Su Z (2006) Crack identification in aluminium plates using Lamb wave signals of a PZT sensor network. *Smart Materials and Structures* 15(3): 839.

Maierhofer C, Myrach P, Reischel M, et al. (2014) Characterizing damage in CFRP structures using flash thermography in reflection and transmission configurations. *Composites Part B: Engineering* 57: 35–46.

Mallat SG and Zhang Z (1993) Matching pursuits with time–frequency dictionaries. *IEEE Transactions on Signal Processing* 41(12): 3397–3415.

Michaels TE, Michaels JE and Ruzzene M (2011) Frequency–wavenumber domain analysis of guided wavefields. *Ultrasonics* 51(4): 452–466.

Mohseni H and Ng C-T (2018) Rayleigh wave propagation and scattering characteristics at debondings in fibre-reinforced polymer-retrofitted concrete structures. *Structural Health Monitoring*. Epub ahead of print 30 January. DOI: 10.1177/1475921718754371.

Moriot J, Quaegebeur N, Duff AL, et al. (2017) A model-based approach for statistical assessment of detection and localization performance of guided wave based imaging

techniques. *Structural Health Monitoring*. Epub ahead of print 4 December. DOI: 10.1177/1475921717744679.

Neerukatti RK, Hensberry K, Kovvali N, et al. (2016a) A novel probabilistic approach for damage localization and prognosis including temperature compensation. *Journal of Intelligent Material Systems and Structures* 27(5): 592–607.

Neerukatti RK, Rajadas A, Borkowski L, et al. (2016b) A hybrid method for damage detection and quantification in advanced X-COR composite structures. In: *Sensors and smart structures technologies for civil, mechanical, and aerospace systems*, Las Vegas, NV, *21–24 March*, p. 980326. Bellingham, WA: SPIE.

Ng WH, Chiam KY and Koh CG (2017) Delta-T acoustic source localization for plate with holes. *Structural Health Monitoring*. Epub ahead print September. DOI: 10.12783/shm2017/14113.

O'Brien TK and Paris IL (2002) Exploratory investigation of failure mechanisms in transition regions between solid laminates and X-cor® truss sandwich. *Composite Structures* 57(1–4): 189–204.

Okabe Y, Fujibayashi K, Shimazaki M, et al. (2010) Delamination detection in composite laminates using dispersion change based on mode conversion of Lamb waves. *Smart Materials and Structures* 19(11): 115013.

Ong WH, Rajic N, Chiu WK, et al. (2017) Lamb wave based detection of a controlled disbond in a lap joint. *Structural Health Monitoring* 17: 668–683.

Peairs DM, Tarazaga PA and Inman DJ (2007) Frequency range selection for impedance-based structural health monitoring. *Journal of Vibration and Acoustics* 129(6): 701–709.

Raghavan A and Cesnik CES (2007) Review of guided-wave structural health monitoring. *Shock and Vibration Digest* 39(2): 91–114.

Revel GM, Pandarese G and Cavuto A (2013) Advanced ultrasonic non-destructive testing for damage detection on thick and curved composite elements for constructions. *Journal of Sandwich Structures & Materials* 15(1): 5–24.

Ruzzene M (2007) Frequency–wavenumber domain filtering for improved damage visualization. *Smart Materials and Structures* 16(6): 2116.

Singh AK, Berggren S, Zhu Y, et al. (2017) Simultaneous strain and temperature measurement using a single fiber Bragg grating embedded in a composite laminate. *Smart Materials and Structures* 26(11): 115025.

Singh AK, Zhu Y, Han M, et al. (2016) Simultaneous load and temperature measurement using Lophine-coated fiber Bragg gratings. *Smart Materials and Structures* 25(11): 115019.

Sohn H, Dutta D, Yang JY, et al. (2011) Delamination detection in composites through guided wave field image processing. *Composites Science and Technology* 71(9): 1250–1256.

Srivastava A and Lanza di Scalea F (2009) On the existence of antisymmetric or symmetric Lamb waves at nonlinear higher harmonics. *Journal of Sound and Vibration* 323(3–5): 932–943.

Su Z and Ye L (2004) Lamb wave based quantitative identification of delamination in CF/EP composite structures using artificial neural algorithm. *Composite Structures* 66(1–4): 627–637.

Su Z, Ye L and Lu Y (2006) Guided Lamb waves for identification of damage in composite structures: a review. *Journal of Sound and Vibration* 295(3): 753–780.

Ulrich TJ (2006) Envelope *c*alculation from the *H*ilbert *t*ransform (technical report). Los Alamos, NM: Los Alamos National Laboratory.

Yu L and Giurgiutiu V (2005) Advanced signal processing for enhanced damage detection with piezoelectric wafer active sensors. *Smart Structures and Systems* 1(2): 185–215.

Zhang G, Wang B, Ma L, et al. (2014) Energy absorption and low velocity impact response of polyurethane foam filled pyramidal lattice core sandwich panels. *Composite Structures* 108: 304–310.